

Fabrication of three-dimensional photonic crystal structures by interferometric lithography and nanoparticle self-assembly

Deying Xia, Jingyu Zhang, Xiang He, and S. R. J. Brueck^{a)}

*Center for High Technology Materials and Department of Electrical and Computer Engineering,
University of New Mexico, 1313 Goddard, SE, Albuquerque, New Mexico 87106, USA*

(Received 10 May 2008; accepted 28 July 2008; published online 20 August 2008)

We report a simple approach to fabrication of three-dimensional photonic crystal structures. One-dimensional photoresist patterns (lines) are defined as templates using interferometric lithography and silica nanoparticles are self-assembled around the photoresist patterns using spin coating. Multiple-layer structures are formed by repeating these processing steps. The photoresist patterns are removed through high temperature calcination to fabricate three-dimensional photonic crystals with void channels in a woodpile structure. The optical properties of as-prepared photonic crystal structures are in good agreement with simulation results. This approach provides a versatile and facile technology to fabricate photonic bandgap materials and photonic crystals with defects.

© 2008 American Institute of Physics. [DOI: 10.1063/1.2971202]

Since the concept of photonic crystals (PCs) was proposed in 1987,^{1,2} the fabrication and application of such structures has attracted an increasing amount of interest. While much effort has been devoted to one-dimensional (1D) (Bragg reflectors) and two-dimensional integrated optics applications, three-dimensional (3D) PCs remain the most challenging to fabricate as well as having unique applications as a result of the 3D photonic confinement. There are two main fabrication approaches: “top-down” lithography and “bottom-up” self-assembly. Top-down approaches utilize sophisticated conventional semiconductor lithography processing, including photolithography, etching, metallization, lift-off, and planarization to fabricate 3D highly periodic structures in a layer-by-layer manner and to accommodate defects (cavities, waveguides, etc.).^{3,4} Contrastingly, self-assembly of colloidal microspheres, provides a simple and inexpensive approach to fabrication of 3D PCs, however, with relatively short range of ordering (grain boundaries) and typically without any capability for programmed defects.^{5,6} In this communication, we present a novel 3D PC fabrication approach using combined top-down [interferometric lithography (IL)] and bottom-up processes (deposition of nanoscale particles from colloidal suspensions) that provide both the long-range order associated with lithography and the ready possibility of introducing controlled pattern defects while retaining the low cost fabrication advantages of self-assembly.

One of most studied PC structures is a “woodpile PC.” Woodpile structures are generally fabricated with intensive top-down methods by layer-by-layer stacking of dielectric rods with alternating orthogonal directions.⁷ A related structure to woodpile PC is a void channel structure where the adjacent void channel layers are separated by a thin solid layer. These woodpile PCs can possess a complete bandgap and offer great flexibility in tuning the photonic bandgap.⁸ While there has been an initial report of the fabrication of woodpile PCs with a dual periodicity using photolithography and self-assembly technique,⁹ the colloidal particle diameters are in the several hundred nanometer range while the peri-

odicity of the patterned strips of colloidal particles is in the 10 μm range. Thus the PC arises from the particle self-assembly and is only weakly impacted by the lithography. In contrast, we use much smaller nanoparticles (~ 50 nm diameter) that form an effective index material ordered by the ~ 500 nm lithography pattern that defines the PC.

We have recently developed a simple templating technology for the formation of various surface patterns of nanoparticles using directed self-assembly, combining top-down IL and bottom-up self-assembly of colloidal particles.^{10,11} We reported a facile approach to fabrication of the porous nanochannels¹² and explored the application for biological separation and detection.¹³ Here, we extend this demonstration to the fabrication of PCs and report on the corresponding optical spectra.

IL can produce simple periodic structures (lines/spaces) at scales across the entire range of interest for PCs and over extended areas (>6 cm^2). IL has been used to generate 3D PCs in single photolithography step using multiple coherent exposure beams, but there are some limitations associated with the difficult phase adjustment between the beams.^{14,15} For woodpile geometries, a layer-by-layer approach is necessary. The interlevel alignment of the fringes with nanoscale accuracy in IL is simple and inexpensive using projection moiré approaches, thus, eliminating the requirement of a high accuracy mask aligner.^{16,17} Compared to e-beam lithography, IL is fast, inexpensive, and provides high uniformity over a large area without stitching artifacts. With IL and layer-by-layer construction, 3D woodpile PCs are readily fabricated using high-refractive-index materials.¹⁸

In our experiments, a quartz slide was used as a substrate for optical transparency and tolerance to high temperature. A uniform silica nanoparticle film was first deposited on a quartz substrate using spin coating.¹⁹ IL was used to produce periodic 1D photoresist (PR) patterns atop the silica nanoparticle film. IL with a 355 nm third-harmonic YAG laser source at a dose of ~ 100 mJ/cm^2 was used to produce 1D periodic patterns. The PR patterns acted as templates for subsequent processing.²⁰ Then, silica nanoparticles were spun onto the PR patterns using nearly monolayer thickness spin-coating cycles, filling the spaces between the PR and forming a uni-

^{a)}Electronic mail: brueck@chtm.unm.edu.

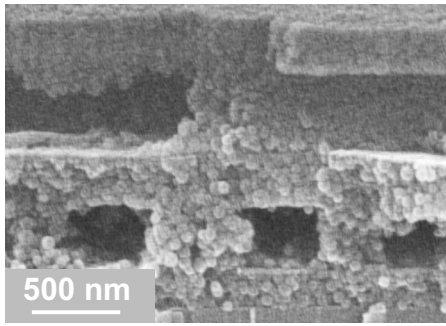


FIG. 1. SEM images of two-layer (x - y) void-channel structures with 1000 nm period and 50 nm diameter silica nanoparticles.

form, low roughness top layer over the PR, which served as the substrate for the next level of the woodpile PC. The 5 wt % concentration, 50 nm silica nanoparticle colloidal suspensions were diluted from Snowtex OL colloid silica obtained from Nissan Chemical American Corp. Several cycles of spin coating with spin speed of 4000 rpm were used. Perpendicular 1D PR patterns were fabricated on this silica nanoparticle surface and deposition of silica nanoparticles to cover the second layer PR patterns was performed using spin coating. Multiple layered structures were generated by repeating the above procedure. Finally, the PC fabrication was completed with a high temperature calcination step (800 °C, air ambient, 2 h) to remove the buried 1D PR patterns and to enhance the mechanical stability of the PC structures by partial necking of the abutting silica nanoparticles while the nanoparticle porosity and the spherical shape of nanoparticles were maintained.¹² Compared with previous fabrication methods for woodpile structures, our approach eliminates many expensive processing steps. The one-step calcination provides a uniformity advantage across the many layers.

Figure 1 shows scanning electron microscopy (SEM) images of a two-layer (x - y) woodpile structure formed with 50 nm silica nanoparticles using negative PR. The rectangular cross sections of the first layer channels end on to the image (around four-particles high) are evident, while the second layer channels are perpendicular to first layer channels. The fracture of the substrate was slightly misaligned relative to the top channel layer, so an interior wall is visible. The channel inside wall is smooth and the channels are continuous. The loose particles in all of the figures are a result of the fracture of the substrate and are not inherent to the fabrication. With this approach, it is easy to fabricate PCs with additional layers, as shown in Fig. 2, for three-layer and four-layer PCs. In these structures, the periodicity appropriate to the PC is set in the transverse directions by the IL and in the vertical directions by the thickness of the PR. The nanoparticles are small compared with the PC dimensions and an effective medium model is appropriate. Sample dimensions were typically ~ 6 cm² with good uniformity across the entire area.

It is easy to vary the PC dimensions using IL. Figure 3 shows the SEM images of four-layer woodpile void nanochannels using positive PR and 50 nm silica nanoparticles on a Si substrate. The period of channels was 500 nm and the space ratio of channels is small due to usage of positive PR. The nanochannel cross section is 150 \times 350 nm². By fracturing a sample in two perpendicular di-

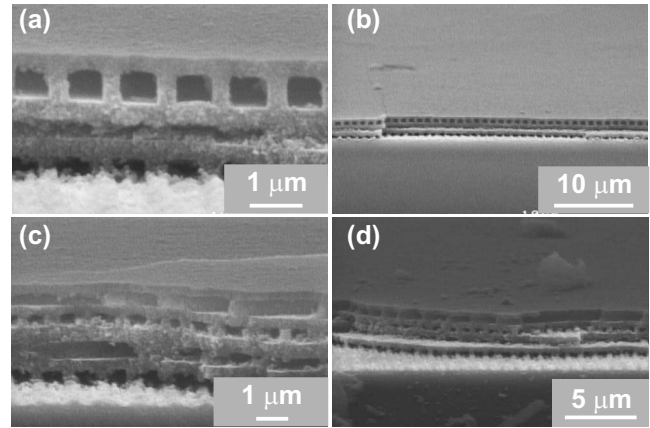


FIG. 2. SEM images of void channel structures with 1000 nm period and 50 nm silica nanoparticles. [(a) and (b)] three-layered structures (x - y - x). [(c) and (d)] four-layered structures (x - y - x - y).

rections, the long-range extent of the pattern is verified in both directions, as shown in Figs. 3(a) and 3(b).

The optical transmission of the as-prepared PC structures (Figs. 1 and 2) for two-layer (x - y), three-layer (x - y - x), and four-layer (x - y - x - y) PCs at normal incidence using a Fourier-transform infrared spectrometer is shown in Fig. 4. The spectrum was normalized to the transmission of a clean quartz substrate. The optical spectrum of a planar silica colloidal nanoparticle film on a quartz substrate was measured for comparison as well. The 2.73 μ m absorption is caused by intrinsic absorption of silica nanoparticles (H₂O) and scales as the total thickness of the nanoparticles. The PC stop bands (transmission minimum) around 2 μ m are clear for these samples. As the number of layers increased, the transmission dip around 2 μ m becomes obvious and shifts to shorter wavelength. The transmission dip for the four-layer PC is around 73%. The transmission dips around 1 μ m for these samples are due to the second-order Bragg diffraction peak. The observed features do not correspond to photonic bandgaps as the dielectric contrast of the silica nanoparticles to the air spaces is too low to provide a complete gap. The silica nanoparticles can be replaced with higher-index nano-

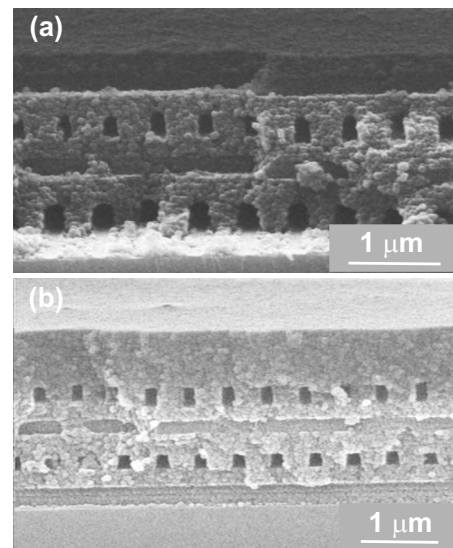


FIG. 3. SEM images of four-layered void channel structures with 500 nm period and 50 nm silica nanoparticles from two different directions.

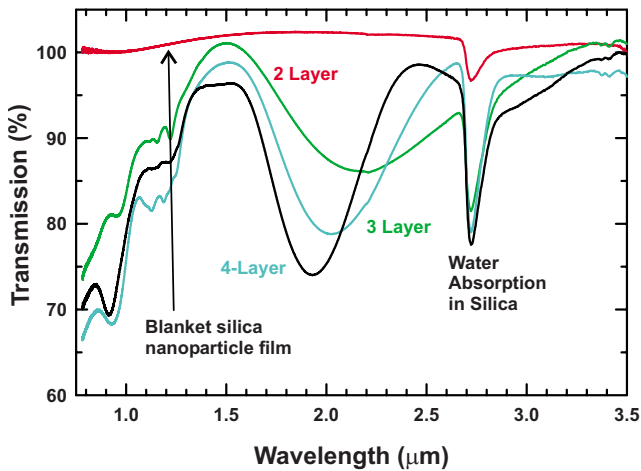


FIG. 4. (Color online) The transmission spectra of the 3D crystals shown in Figs. 1 and 2 measured with FTIR from silica nanoparticle film, two-layer, three-layer, and four-layer PCs. The three main dips are from intrinsic absorption (H_2O) in the silica nanoparticles ($2.73 \mu\text{m}$), stop band ($2 \mu\text{m}$), and second-order Bragg diffraction ($1 \mu\text{m}$).

particles to enhance the photonic behavior such as TiO_2 ,²¹ or metallic nanoparticles.²²

The experimental transmission measurement is complemented by simulation using a rigorous coupled-wave analysis (RCWA) model.²³ The basic idea of RCWA is to expand the dielectric function of the structure into a spatial Fourier series that couples the terms of the Floquet electromagnetic field expansion.²⁴ The effective refractive index of silica nanoparticle film can be estimated by²⁵ $n_{\text{eff}} = \sqrt{f_1 n_1^2 + (1-f_1)n_2^2}$, where n_1 and n_2 are the refractive index of component 1 and 2, respectively, and f_1 is the filling volume fraction of component 1. For the silica nanoparticle regions, $n_{\text{SiO}_2} = 1.45$ and $n_{\text{air}} = 1.00$, f_1 is 0.74 for ideal dense packing of spherical particles and the effective refractive index is $n_{\text{eff}} \sim 1.34$. The curves in Fig. 5 show the RCWA-simulated transmission for three-, four- and eight-layer PCs. The simulated results agree reasonably well with the experimental spectra for the three- and four-layer samples. The strength of the transmission dip increases with the number of layers; 40% transmission is calculated for an eight-layer structure.

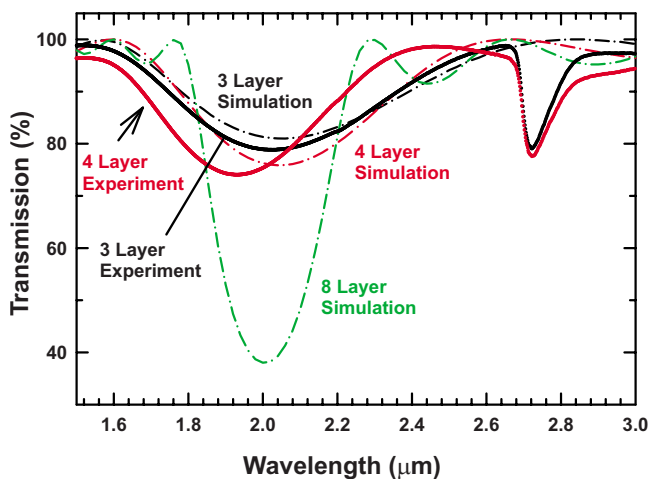


FIG. 5. (Color online) Experimental and RCWA-simulated transmission spectrum at normal incidence.

This approach can easily extend to further fabrication of artificial defects in 3D PCs through introducing extrinsic point, linear, and planar defect patterns in the formation of the PR pattern, combining IL, and conventional optical lithography, or in the self-assembly or using a second type of nanoparticle film layer for a portion of selected layers.²⁶ Our fabricated PCs have potential applications for sensing materials because of their inherent optical properties and dual porosities (channels and voids among nanoparticles).

In summary, we have demonstrated a simple and inexpensive approach for fabricating 3D woodpile PC structures with void channels using interference lithography and self-assembly of nanoparticles. The morphology of PC structures is easily tunable in the lithography and spin-coating steps. The as-prepared photonic structures exhibit interesting optical behavior that agrees well with model results. The complete bandgaps will be achieved through using of high refractive index nanoparticles and the void channel structures may have technical importance for fluid sensing.

This work was supported by DARPA under the University Photonics Research Center program. Facilities of the NSF-sponsored NNIN node at the University of New Mexico were used for the fabrication.

¹E. Yablonovitch, *Phys. Rev. Lett.* **58**, 2059 (1987).

²S. John, *Phys. Rev. Lett.* **58**, 2486 (1987).

³S. Y. Lin, J. G. Fleming, D. L. Hetherington, B. K. Smith, R. Biswas, K. M. Ho, M. M. Sigalas, W. Zubrzycki, S. R. Kurtz, and J. Bur, *Nature (London)* **394**, 251 (1998).

⁴M. Qi, E. Lidorikis, P. T. Rakich, S. G. Johnson, J. D. Joannopoulos, E. P. Ippen, and H. I. Smith, *Nature (London)* **429**, 538 (2004).

⁵Y. A. Vlasov, X. Z. Bo, J. C. Sturm, and D. J. Norris, *Nature (London)* **414**, 289 (2001).

⁶C. Lopez, *Adv. Mater. (Weinheim, Ger.)* **15**, 1679 (2003).

⁷S. Y. Lin, J. G. Fleming, R. Lin, M. M. Sigalas, R. Biswas, and K. M. Ho, *J. Opt. Soc. Am. B* **18**, 32 (2001).

⁸M. J. Ventura, M. Straud, and M. Gu, *Appl. Phys. Lett.* **82**, 1649 (2003).

⁹Q. Yan, X. S. Zhao, J. H. Teng, and S. J. Chua, *Langmuir* **22**, 7001 (2006).

¹⁰D. Xia, A. Biswas, D. Li, and S. R. J. Brueck, *Adv. Mater. (Weinheim, Ger.)* **16**, 1427 (2004).

¹¹D. Xia and S. R. J. Brueck, *Nano Lett.* **4**, 1295 (2004).

¹²D. Xia and S. R. J. Brueck, *J. Vac. Sci. Technol. B* **23**, 2694 (2005).

¹³D. Xia, T. C. Gamble, E. A. Mendoza, S. J. Koch, X. He, G. P. Lopez, and S. R. J. Brueck, *Nano Lett.* **8**, 1610 (2008).

¹⁴M. Campbell, D. N. Sharp, M. T. Harrison, R. G. Denning, and A. J. Turberfield, *Nature (London)* **404**, 53 (2000).

¹⁵X. Wang, J. F. Xu, H. M. Su, Z. H. Zeng, Y. L. Chen, H. Z. Wang, Y. K. Pang, and W. Y. Tam, *Appl. Phys. Lett.* **82**, 2212 (2003).

¹⁶S. R. J. Brueck, *Proc. IEEE* **93**, 1704 (2005).

¹⁷A. Feigel, Z. Kotler, and B. Sfez, *Opt. Lett.* **27**, 746 (2002).

¹⁸A. Feigel, M. Veinger, B. Sfez, A. Arsh, M. Klebanov, and V. Lyubin, *Appl. Phys. Lett.* **83**, 4480 (2003).

¹⁹D. Xia, D. Li, K. Zu, Y. Luo, and S. R. J. Brueck, *Langmuir* **23**, 5377 (2007).

²⁰D. Xia, D. Li, Y. Luo, and S. R. J. Brueck, *Adv. Mater. (Weinheim, Ger.)* **18**, 930 (2006).

²¹S. Colodrero, M. Ocana, and H. Miguez, *Langmuir* **24**, 4430 (2008).

²²J. G. Fleming, S. Y. Lin, I. El-Kady, R. Biswas, and K. M. Ho, *Nature (London)* **417**, 52 (2002).

²³M. G. Moharam, D. A. Pommet, E. B. Grann, and T. K. Gaylord, *J. Opt. Soc. Am. A* **12**, 1077 (1995).

²⁴B. K. Minhas, W. Fan, K. Agi, S. R. J. Brueck, and K. J. Malloy, *J. Opt. Soc. Am. A* **19**, 1352 (2002).

²⁵Y. Xu, X. Zhu, Y. Dan, J. H. Moon, V. W. Chen, A. T. Johnson, J. W. Perry, and S. Yang, *Chem. Mater.* **20**, 1816 (2008).

²⁶Q. Yan, L. Wang, and X. S. Zhao, *Adv. Funct. Mater.* **17**, 3695 (2007).